Biochimica et Biophysica Acta 1797 (2010) 20–28

Contents lists available at ScienceDirect

Biochimica et Biophysica Acta

journal homepage: www.elsevier.com/locate/bbabio

# A novel functional element in the N-terminal region of *Arum concinnatum* alternative oxidase is indispensable for catalytic activity of the enzyme in HeLa cells

Yusuke Kakizaki [a], Roger S. Seymour [b], Kikukatsu Ito [a,*]

[a] *Cryobiofrontier Research Center, Faculty of Agriculture, Iwate University 3-18-8 Ueda, Morioka, Iwate 020-8550, Japan*
[b] *Ecology and Evolutionary Biology, University of Adelaide, Adelaide, South Australia, Australia*

ARTICLE INFO

*Article history:*
Received 1 May 2009
Received in revised form 14 July 2009
Accepted 21 July 2009
Available online 28 July 2009

*Keywords:*
Alternative oxidase
Arum lily
Thermogenesis
Inactive isoform
N-terminus
Loss of function

ABSTRACT

Alternative oxidase (AOX) is a quinol-oxygen oxidoreductase, which is known to possess a dicarboxylate diiron reaction center held in structurally postulated α-helical bundle. However, little is known about the structural or functional features of its N-terminal region in any organism, with the exception of a regulatory cysteine residue (CysI) in angiosperm plants. Here, we show that transcripts of two AOX1 isozymes (*AcoAOX1a* and *AcoAOX1b*) are coexpressed in thermogenic appendices of *Arum concinnatum*, while their enzymatic activities seem to be distinct. Namely, *AcoAOX1a*, an abundantly expressed transcript in vivo, shows an apparent cyanide-insensitive and *n*-propyl gallate-sensitive respiration during ectopic expression of the protein in HeLa cells, whereas *AcoAOX1b* exhibits a lower transcript expression, and appears to be totally inactive as AOX at the protein level. Our functional analyses further reveal that an E83K substitution in AcoAOX1b, which is located far upstream of CysI in the N-terminal region, is the cause of this loss of function. These results suggest the presence of a naturally occurring inactive AOX homologue in thermogenic plants. Accordingly, our results further imply that the N-terminal region of the AOX protein functionally contributes to the dynamic activities of respiratory control within the mitochondria.



## 1. Introduction

Alternative oxidase (AOX) of eukaryotic taxa is a terminal quinol oxidase of mitochondrial electron transport chains, which catalyzes the oxidation of ubiquinol and the four-electron reduction of molecular oxygen to water in a coupling manner [1]. Unlike cytochrome *c* oxidase (COX), AOX does not translocate protons across the inner mitochondrial membrane, thus, no redox energy is conserved into the electrochemical proton gradient by this enzyme. Despite such a dissipative nature in energy metabolism, there have been a number of reports suggesting that AOX plays a variety of physiological roles in higher plants, for example, contribution to floral thermogenesis [2], alleviation of reactive oxygen species (ROS) formation [3,4] and maintenance of TCA cycle turnover under restriction of COX-mediated respiration [5]. In fact, recent work on thermogenic receptacles of sacred lotus (*Nelumbo nucifera*) has shown that an increase in respiration through AOX is largely responsible for an increase in heat production [6].

Comparative analyses and site-directed mutagenesis studies have been successful in elucidating the structural and mechanistic nature of AOX, although no data from X-ray crystallography are available for analysis to date. Andersson and Nordlund presented a structural model of AOX in which they postulated four α-helices and two possible membrane binding domains [7]. In this model, they also proposed ligands to a catalytic diiron center in analogy with other diiron carboxylate proteins. A number of site-directed mutagenesis studies have confirmed that all of these iron binding residues are necessary for AOX activity, except for the glutamic acid in the first helix region [1,8,9]. Besides the active center, two highly conserved cysteines in plant AOX, termed CysI and CysII [10], have received attention. These cysteines are considered to play key roles in post-translational regulatory systems of AOX, namely redox regulation and activation by α-keto acids. Previous investigations have revealed that CysI is responsible not only for formation of disulfide bonds for redox regulation, but also for interaction with α-keto acids such as pyruvate, whereas CysII can act only as a target of activation by small α-keto acids, such as glyoxylate [11–13]. The AOX activity is, indeed, largely affected by these post-transcriptional regulation mechanisms, both in vivo and in vitro.

Mutagenesis studies have demonstrated that a single amino acid substitution in AOX drastically alters its enzymatic characteristics. For instance, substitutions of CysI by charged amino acids results in remarkably increased basal activity and insensitivity to pyruvate [13] while the substitution by serine yields an enzyme that is activated by succinate but not by pyruvate [14,15]. Another representative case of a single substitution having a large impact is reported in the G303E mutant of *Arabidopsis thaliana* AOX, which shows a 4.6-fold increase in resistance to salicylhydroxamic acid (SHAM) [16], a specific inhibitor of AOX. Site-directed mutagenesis studies with respect to

* Corresponding author. Tel./fax: +81 19 621 6143.
*E-mail address:* kikuito@iwate-u.ac.jp (K. Ito).

0005-2728/$ – see front matter 
doi:10.1016/j.bbabio.2009.07.006

potential catalytic mechanisms of AOX also revealed several residues that have impacts on the enzymatic activity both in plant AOXs [9,17] and in typanosomal AOXs (TAOs) [18].

With such a great deal of experimental effort, there has been notable progress in our understanding of the structure–function relationships of AOX, however, little is known about the biochemical characteristics of its N-terminal region other than the CysI residue. In this study, we demonstrate that a single amino acid substitution (E83K) in the N-terminal region causes a loss of activity in AOX from *Arum concinnatum*, whose intense thermogenic activity was recently discovered [19] but has not been investigated at the molecular level to date. This substitution seems to occur naturally in a pair of AOX isozymes in thermogenic appendices of this plant. Our findings suggest that an additional element in the N-terminal region is essential for the activity of AOX, and a translation product which shows homology to known AOXs may not always be functionally active within the mitochondria.

## 2. Materials and methods

### 2.1. Plant materials

*A. concinnatum* from a population near Panormos, a village on Crete, an island of Greece, were observed in the field for characterizing their thermogenic and morphological properties. Tissue samples for RNA extraction were collected from the plants grown in a population near the campus of University of Crete in Heraklion. All samplings and observations were conducted in May 2007.

### 2.2. Thermal imaging and temperature measurement

To verify thermogenicity of *A. concinnatum*, thermal images were obtained using Avio TVS-500 infrared camera (Nippon Avionics Co, Ltd., Tokyo, Japan) then saved as IRI files. The IRI images were subsequently analyzed with Goratec Thermography Studio Professional software (Goratec Technology GmbH and Co., KG, Erding, Germany). The temperatures were measured with copper-constantan thermocouples in the air and in the appendix. They were recorded with Grant Squirrel data logger (Grant Instruments, Cambridge, UK).

### 2.3. Isolation and sequencing of the full-length AcoAOX1a and AcoAOX1b

For the isolation of transcripts encoding AOX proteins by RT-PCR, total RNA was first extracted using an RNeasy Plant Mini Kit (Qiagen, Venlo, Netherlands) from thermogenic appendix samples that had been flash-frozen in liquid nitrogen in the field, immediately after sampling. First strand cDNAs were generated with a PrimeScript 1st strand cDNA Synthesis Kit (TaKaRa Bio Inc., Otsu, Japan) using an oligo (dT) primer. By aligning conserved cDNA sequences of *AOX* transcripts across several aroid species, namely *Dracunculus vulgaris AOX* [20], *Philodendron bipinnatifidum AOX* [20] and *Sauromatum guttatum AOX* [21], primers were designed to amplify approximately 550 bp fragments from the ORF region (Step 1 in Fig. S1): AcoPartF1 and AcoPartR1 (for all primer and probe sequences, see Table 1). The fragments were cloned into pCR 2.1 with a TA Cloning Kit (Invitrogen, Carlsbad, CA, USA), then sequenced.

Based on the partial sequence data, 5′- and 3′-RACE reactions were performed using a SMART RACE cDNA Amplification Kit (Clontech Laboratories Inc., Palo Alto, CA, USA) with these primers (Step 2 in Fig. S1): AcoRV2 and AcoRV1 for the *AcoAOX1a* 5′-fragment, AcoFW1 for the *AcoAOX1a* 3′-fragment, AcoF3re and AcoF2re for the *AcoAOX1b* 5′-fragment and AcoFW5 and AcoR4re for the *AcoAOX1b* 3′-fragment. Nested PCR was conducted when necessary. As both of AcoAOX1a- and AcoAOX1b-derived products had been amplified simultaneously with the primers, AcoAOX1b 5′- and 3′-fragments were screened by restriction enzymes *Ava*I and *Bst*XI (both from TaKaRa Bio Inc.), respectively. RACE products were also cloned into pCR2.1 and sequenced.

**Table 1**
Primer and probe sequences used for RT-PCR and real-time PCR.

| Name | Sequence (5′ to 3′) |
|---|---|
| AcoPartF1 | GCCCCCACCACCATCCTCGACA |
| AcoPartR1 | TCGCGGTGGTGTGCCTCGTCGG |
| AcoRV2 | ACCGCCGCCACCGTCTCCA |
| AcoRV1 | TGTACAAGGCCAGCTTGTCGAGGACGGT |
| AcoFW1 | CCGGGCGATGATGCTGGAGA |
| AcoF3re | AACTCGGTGTAGGAGTGGATGGCCTCCT |
| AcoF2re | ACCCGGTGGGCGAACTTGGGGGAGA |
| AcoFW5 | TGCCGGGCGATGATGCTGGAGA |
| AcoR4re | AGAACGAGCGGATGCACCTGATGACCTT |
| Aco5′E | ACGATCGAAGGAGCCAGTGCAGT |
| Aco3′A | TAGAGTTCGCCAGTAGTAATGCTAATGCGT |
| Aco5′C | AGCCAGTGCAGTCCCCT |
| Aco3′C | TTCCCACTGTGGATTCACGTGAA |
| SalI-Aco5′ | CTGCAGGTCGACAGCACGCTGTCAGATCCCGCCCA |
| SalI-Aco3′ | CTCGAGGTCGACTGGATTCACGTGAAGCCTCCGCGCT |
| efFW1 | ACATTGTGGTCATTGGCCA |
| efRV3 | ACCAGTTGGGTCCTTCTT |
| Aco1aF | TTCCTCGGGTACCTCATC |
| Aco1aR | GGCACGTTCTCGATGGTG |
| Aco1bF | GGGGCCATCCAGGACAC |
| Aco1bR | GTCCGAGGCGAAATGGT |
| ef1aF | ACGGTTATGCTCCTGTCCT |
| ef1aR | TTCAAGAACTTGGGCTCCT |
| Aco1aP | AGATCGACAAGG |
| Aco1bP | CGAGGGCGAT |
| ef1aP | TGACGAAGATCG |

For the probes, positions at which RNA nucleotides are allocated are indicated by underbars.

To obtain full-length cDNAs of *AcoAOX1a* and *AcoAOX1b*, another PCR amplification was performed using KOD -Plus- (TOYOBO Co., Ltd., Osaka, Japan) with Aco5′E and Aco3′A primers for the first reaction, followed by Aco5′C and Aco3′C primers for the nested PCR (Step 3 in Fig. S1). The final PCR products of almost 1.2 kb were purified by gel extraction, then cloned into the *Hinc*II site of pUC118 (TaKaRa Bio Inc.) following phosphorylation by calf intestinal alkaline phosphatase (New England Biolabs, Inc., Ipswich, MA, USA). The molecular species of the insert, i.e. either *AcoAOX1a* or *AcoAOX1b*, was identified by applying *Ava*I to PCR products amplified from each single clone with AcoF3re and AcoR4re primers before they were sequenced (Step 4 in Fig. S1). Nucleotide sequence data were analyzed with GENETYX software (Genetyx Corp., Tokyo, Japan). Phylogenetic analysis was conducted with MEGA version 4 [22].

### 2.4. Construction of vectors

DNA fragments that carry sequences corresponding to the mature forms of the AcoAOXs were amplified with SalI-Aco5′ and SalI-Aco3′ primers, following prediction of their mitochondria targeting sequences with Mitoprot [23]. The fragments were then digested with *Sal*I restriction enzyme to be cloned into *Sal*I site of pCMV/myc/mito (Invitrogen).

To construct vectors for expression of chimera proteins, the vectors carrying wild-type AcoAOX inserts were digested sequentially with *Ksp*I, *Eco*RI and *Nar*I (*Ksp*I and *Nar*I from Roche Diagnostics GmbH, Mannheim, Germany; *Eco*RI from TaKaRa Bio Inc.). The starting plasmid linearized with *Ksp*I was digested firstly with *Eco*RI to cleave at the middle of the inserts, and the fragments that contain sequences encoding N-terminal domain were subsequently digested with *Nar*I to generate further segmented inserts. The fragments were re-associated in appropriate combinations to generate the designed chimeric inserts. Ligation reactions were performed with a TaKaRa DNA Ligation Kit Ver.2.1 (TaKaRa Bio Inc.). During the construction of the expression plasmids, an additional IHSLLQVD sequence was added

to the N-terminus of each mature product. All the plasmid vectors were purified with an Endofree Plasmid Maxi or Mega Kit (Qiagen) then sequenced from the bovine growth hormone polyadenylation signal (BGH) reverse priming site downstream of the cloning site.

### 2.5. Transfection of HeLa cells

On a day prior to transfection treatments, $3.0 \times 10^6$ cells were plated in 10 cm-dish containing 10 mL of Dulbecco's Modified Eagle Medium (DMEM: Invitrogen) with 1 mM pyruvate, 10 mM galactose, 5 mM HEPES, 6 mM glutamine and Cellect fetal bovine serum (MP Biomedicals Inc., Solon, OH, USA). Plasmids were transfected into the HeLa cells using Lipofectamine 2000 (Invitrogen) at a 4:1 weight ratio with a transgenic marker, a nucleus localizing red fluorescent protein pDsRed2-Nuc (Clontech Laboratories Inc.). Twenty-four hours after the transfection, the cells were trypsinized and suspended in 1.4 mL DMEM without pyruvate. Using 200 μL of the suspended cells, the intensity of DsRed2 fluorescence was detected with FACScan (Becton, Dickinson and Company Inc., Franklin Lakes, NJ, USA) according to the manufacturer's instructions, and transfection efficiency was calculated (data not shown).

### 2.6. Measurement of oxygen consumption

Oxygen consumption rates of the suspended cells prepared as described above were measured using a Clark-type electrode (Oxy1, Hansatech Instrument Inc., King's Lynn, Norfolk, UK) at 37 °C according to previously reported methods [4].

### 2.7. Subcellular localization and Western blotting

For sample preparations, the suspended cells for which oxygen consumption rates had been measured were washed several times in PBS buffer and then centrifuged to remove any trace of the buffer. The pelleted cells were stored at −30 °C until they were used. To analyze the subcellular localization of transfected gene products, cells were fractionated using a Subcellular Proteome Extraction Kit (Calbiochem Inc., San Diego, CA, USA). After concentration of fractioned proteins by acetone precipitation, 15 μg of each sample was used for the subsequent Western blotting as previously described [4].

### 2.8. Expression analysis of AcoAOX1a and AcoAOX1b

To carry out relative quantification of *AcoAOX1a* and *AcoAOX1b* with a real-time PCR system, a partial fragment that encodes *EF1α* was isolated from a thermogenic appendix sample of *A. concinnatum* (DDBJ accession number AB485995). A set of efFW1 and efRV3 primers amplified an approximately 1.3 kb fragment, which was then cloned into pCR2.1 and sequenced. cDNAs for real-time PCR analyses were prepared by the method described in the previous section 2.3.

To detect the amplification specifically derived from a single transcript, cycling probe technology [24,25] was adopted with these gene-specific primers (Fig. S3): Aco1aF and Aco1aR for *AcoAOX1a*, Aco1bF and Aco1bR for *AcoAOX1b* and ef1aF and ef1aR for *AcoEF1α*. With these primers, specifically amplified products were produced and detected with real-time PCR, using probes that had also been designed specifically for each transcript. Aco1aP, Aco1bP and ef1aP are the probes for *AcoAOX1a*, *AcoAOX1b* and *AcoEF1α*, respectively. All reactions were performed in the same conditions with a CycleavePCR Core Kit (TaKaRa Bio Inc.) using a Thermal Cycler Dice Real Time System (TaKaRa Bio Inc.). Conditions for the reaction were as follows: 94 °C for 10 s, 60 cycles of 95 °C for 5 s, 65 °C for 15 s and 72 °C for 30 s. Expression quantity of the respective transcripts was analyzed with corresponding plasmid standards, and the quantitative ratio of either *AcoAOX* to *AcoEf1α* was compared to that of its counterpart to *AcoEf1α*.

### 2.9. Statistical analyses

Error bars represent standard deviations from the mean. *F*-tests for homogeneity of variance were performed, followed by appropriate *t*-tests for comparison of two means.

## 3. Results

### 3.1. Thermogenesis in A. concinnatum

A thermal image of the aerial part of *A. concinnatum* whose spathe had fully opened indicated that surface temperature of its appendix tissue was higher than ambient temperature (Fig. 1A). The maximum

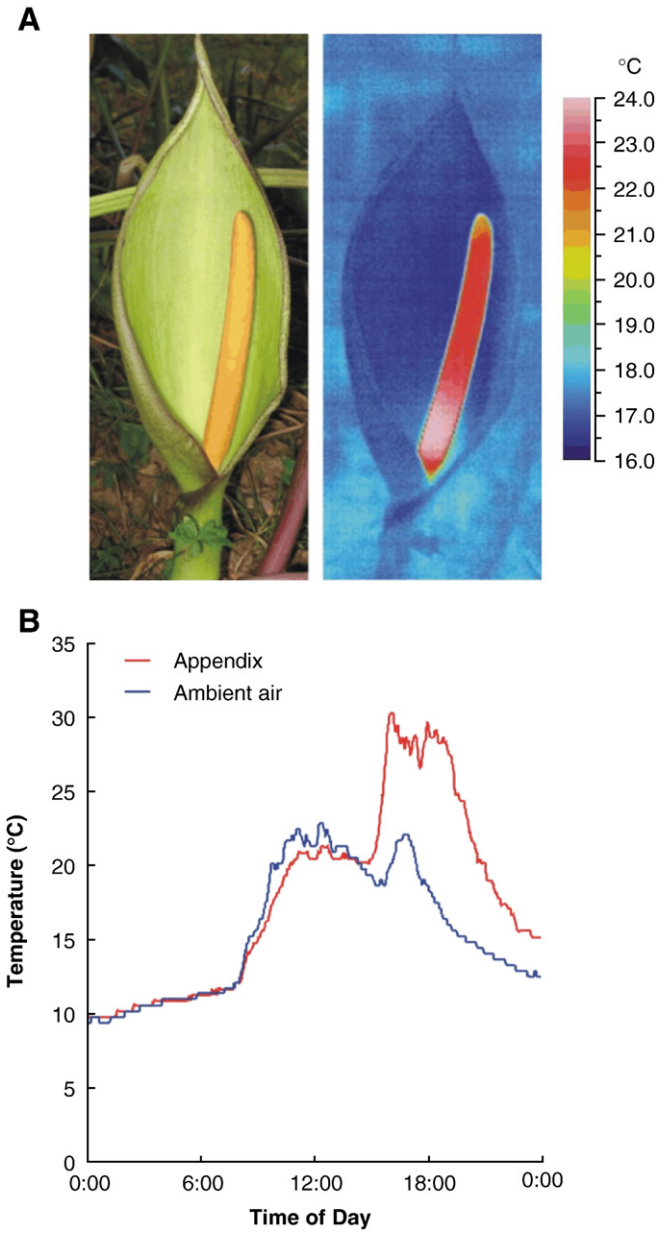


**Fig. 1.** Thermogenesis of *Arum concinnatum*. (A) Structural features of an *A. concinnatum* inflorescence in which the greenish spathe has opened to reveal the thermogenic appendix (left), and a thermographic image captured from the same angle with a high-resolution infrared camera (right). The temperature scale of the thermographic analysis is shown on the right. (B) Temperature time course of the intact appendix and ambient air during thermogenesis. The data were collected continuously over 24 h.

appendix temperature was about 30 °C, while the ambient temperature was 20 °C (Fig. 1B).

Aside from measurements of temperature, there were morphological changes in the inflorescences that are associated with thermogenesis, as in other aroid species [26–28]. The spathe that initially encloses the inflorescence opens at onset of the thermogenesis, and the appendix remains erect throughout the thermogenic stage. On proceeding to the post-thermogenic stage, the appendix and spathe begin to wilt. These morphological features were used as indicators of physiological stages of thermogenesis for tissue samples.

### 3.2. Isolation of homologous AOX transcripts

RT-PCR based cloning of AOX transcripts was performed on total RNA extracts from thermogenic appendices. As two homologous partial fragments of *AOX* transcripts were detected on several independent amplifications of identical cDNA templates, full-length cDNAs of the corresponding transcripts were isolated and consequently named *AcoAOX1a* and *AcoAOX1b* (DDBJ accession numbers AB485993 and AB485994, respectively). Phylogenetic analysis of *AcoAOX1a* and *AcoAOX1b* with thirteen other nucleotide sequences of AOX homologues showed that both of them encoded different AOX1-type isoforms (Fig. S3).

Alignment of the deduced amino acid sequences revealed that they shared approximately 95.4% identity with each other (Fig. 2). Both of them contained structural and functional characteristics of typical plant AOXs, such as four α-helical bundles, ligands for two iron atoms of the active center and two regulatory cysteine residues [17]. Mitoprot predicted a common cleavage site of mitochondrial targeting sequences for both AcoAOX1a and AcoAOX1b that would produce the mature proteins of 31.9 kDa and 31.7 kDa, respectively.

### 3.3. Functional analysis of AcoAOX1a and AcoAOX1b

We have previously developed a heterologous expression system for a plant AOX using HeLa cells, an immortal cell line derived from human cervical cancer cells [4]. To perform functional analysis of the AcoAOXs in this system, expression vectors were constructed that carry sequences corresponding to the mature forms of the respective AcoAOX isoforms downstream of a human mitochondrial targeting sequence (Fig. 3A).

Cellular oxygen consumption conferred by the AOX pathway was measured (Fig. 3B), as it was considered to reflect activities and characteristics of the introduced AOXs. For the mock control and the cells transfected with the empty vector, addition of 1 mM KCN, an inhibitor of complex IV, substantially inhibited their basal oxygen consumption, which was affected by neither addition of 1 mM pyruvate, an activator of typical plant AOXs, nor addition of 0.1 mM *n*-propyl gallate (nPG), a specific inhibitor of the AOXs. The cells expressing AcoAOX1a clearly exhibited cyanide-resistant oxygen consumption, which was further activated by addition of pyruvate and subsequently inhibited in the presence of nPG. On the other hand, the cells expressing AcoAOX1b showed little cyanide-resistant oxygen consumption and rather behaved like the empty vector control.

Oxygen consumption capacities after respective drug additions were calculated on the basis of the oxygen consumption level at the basal condition (Fig. 3C). The capacity of AcoAOX1a-expressing cells in the presence of KCN was as high as 21.7 ± 2.3% of the basal consumption, and significantly higher than that of the mock control, vector control and AcoAOX1b-expressing cells. Also, it appeared that the sequential drug additions in the presence of KCN had a significant effect only on AcoAOX1a-expressing cells.

Expression level and subcellular localization of the AcoAOX proteins were analyzed with Western blotting (Fig. 3D). Both of the expressed AcoAOX proteins were confirmed to be co-fractioned with the mitochondrial marker protein, complex III core 2 subunit, but not with the cytosolic marker protein, μ-calpain. Their intracellular accumulation levels were almost equivalent to each other, however, AcoAOX1b showed a tendency to be expressed at a slightly lower level than AcoAOX1a. Although mobility of the proteins on SDS-PAGE had been predicted to show little difference according to their deduced amino acid sequences, their molecular mass was different, relative to


**Fig. 2.** Primary structures of AcoAOXs. Deduced amino acid sequences of the two *A. concinnatum* AOX proteins, AcoAOX1a and AcoAOX1b, and their predicted structural features. Red bold characters highlight mismatched residues between the two sequences. A green polygonal arrow represents the putative cleavage site of their mitochondrial targeting sequences according to Mitoprot. Regulatory cysteine residues and iron binding ligands are denoted by blue asterisks and black arrowheads, respectively. Four α-helical regions proposed in the current AOX model are indicated by gray underlines.

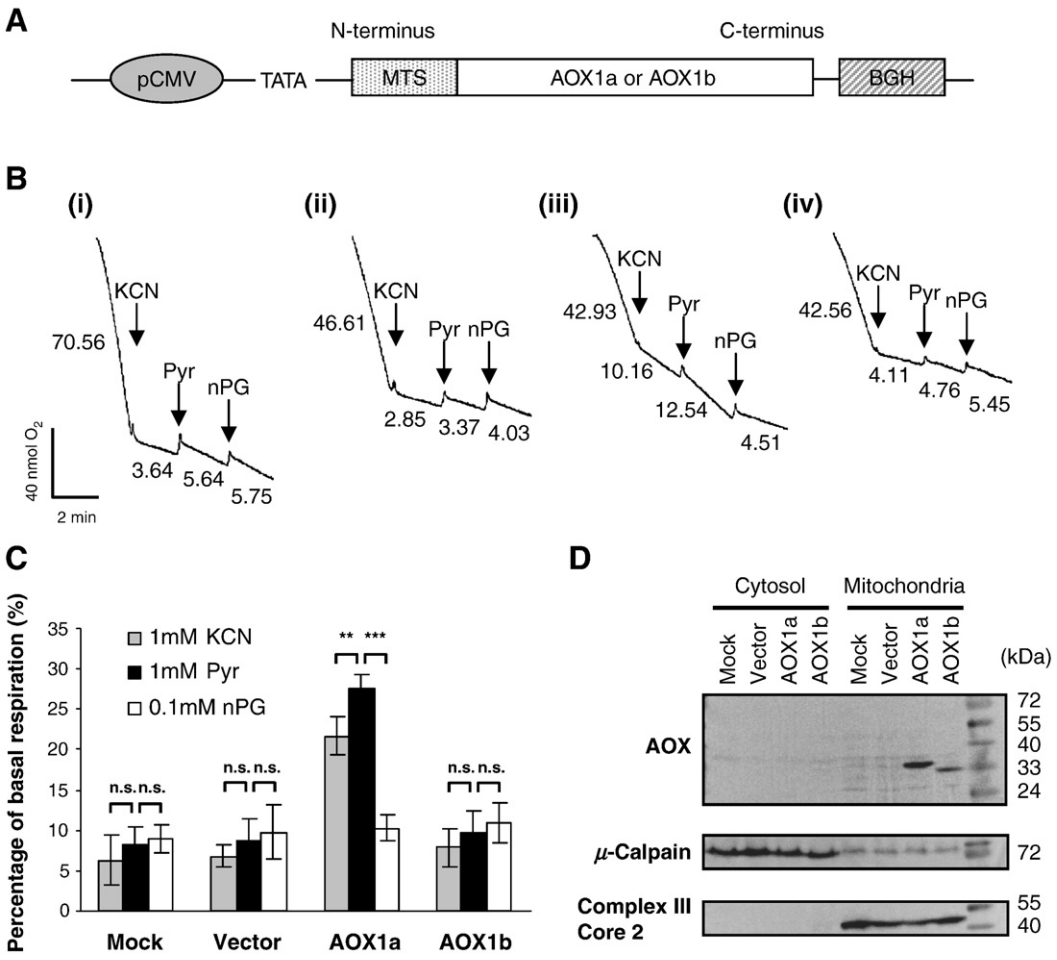


**Fig. 3.** Effect of AcoAOX1a and AcoAOX1b expressed in HeLa cells on their respiratory properties. (A) Schematic representation of an expression construct that carries a sequence corresponding to the predicted mature form of respective AOX proteins fused with a mitochondrial targeting sequence (MTS) from subunit VIII of human cytochrome *c* oxidase. The constructs which express AcoAOX1a and AcoAOX1b are hereafter referred to as AcoAOX1a and AcoAOX1b, respectively. Abbreviations are as follows: pCMV; immediate-early cytomegalovirus promoter, TATA; TATA box, BGH; bovine growth hormone polyadenylation signal. (B) Typical oxygen uptake activity of HeLa cells without transfection treatment, i.e. mock control (i), and those transfected with vector (ii), AcoAOX1a (iii) and AcoAOX1b (iv). Where indicated, the following additions were made: 1 mM KCN, 1 mM Pyruvate (Pyr) and 0.1 mM *n*-propyl gallate (nPG). Numbers along the traces refer to oxygen consumption rates (nmol $O_2^{-1}$ $min^{-1}$ per dish culture). Scale bars are shown at the bottom left. The graph is representative of four independent experiments. (C) Respiration capacities of the cells on respective drug additions described above. The capacities were obtained by calculating ratios of respiration rates on each drug addition to those at the basal conditions. A mock control sample is abbreviated as Mock, and samples of the cells transfected with vector, AcoAOX1a and AcoAOX1b are labeled as Vector, AOX1a and AOX1b, respectively. Significance of *t*-test is indicated as follows: $^{**}P<0.01$, $^{***}P<0.001$ and n.s. not significant. (D) Western blotting of subcellular fractions extracted from the HeLa cells. The fractions were separated by SDS-PAGE under non-reducing conditions, then immunoblotted with AOA monoclonal antibody raised against *S. guttatum* AOX, which can cross-react with a variety of heterogenous AOX proteins [29,30], followed by anti-μ-calpain antibody as a cytosolic marker and anti-complex III core 2 subunit antibody as a mitochondrial marker. A protein standard is indicated at the right of the image along with the corresponding molecular mass in kDa.

the protein standard. AcoAOX1a was detected at 34.7 kDa, which was larger than its predicted molecular mass of 32.8 kDa, while AcoAOX1b was at 32.5 kDa which is practically equal to its predicted molecular mass of 32.6 kDa.

### 3.4. Mutational analysis of AcoAOXs using chimeric proteins

To deduce specific position(s) of the residue(s) responsible for the loss or gain of function in AcoAOXs, two chimeric proteins (Fig. 4A), chimera 1 and chimera 2, were expressed in the HeLa cells. The chimera 1 possessed the primary structure of the N-terminus of AcoAOX1a and the C-terminus of AcoAOX1b, while this structure was reversed in chimera 2. The two components were fused at the end of the second α-helical region where corresponding nucleotide sequences were highly conserved between them.

Comparing oxygen consumption capacities of the chimera 1- and chimera 2-expressing cells along with those of the mock control and the empty vector control (Fig. 4B), the chimera 1-expressing cells exhibited significantly higher levels of cyanide-resistant oxygen consumption, while the chimera 2-expressing cells failed to sustain it at a significant level. This cyanide-resistant oxygen consumption of the chimera 1-expressing cells could be further stimulated drastically by pyruvate and inhibited by subsequently added nPG. The degree of this pyruvate-induced activation was 233.3 ± 19.5%, which was about twice as high as that of AcoAOX1a-expressing cells (128.3 ± 6.8%).

The results from the functional analysis of chimera 1 and chimera 2 proteins indicated possible involvement of any or all of the three amino acid substitutions in the N-terminal region, i.e. the 83rd, 110th and 130th positions, in influencing nature of the AOX activity. Therefore, additional two chimeric proteins, chimera 3 and chimera 4, were constructed to further narrow down the candidate substitutions (Fig. 4A). Chimera 3 had the sequence of AcoAOX1b in the region up to and including residue 83 and the sequence of AcoAOX1a in the region covering residues 110 and 130, while chimera 4 contained the opposite construct.

Oxygen consumption capacities of the chimera 3- and chimera 4-expressing cells illustrated the expected functional difference between these proteins (Fig. 4B). While the chimera 3-expressing

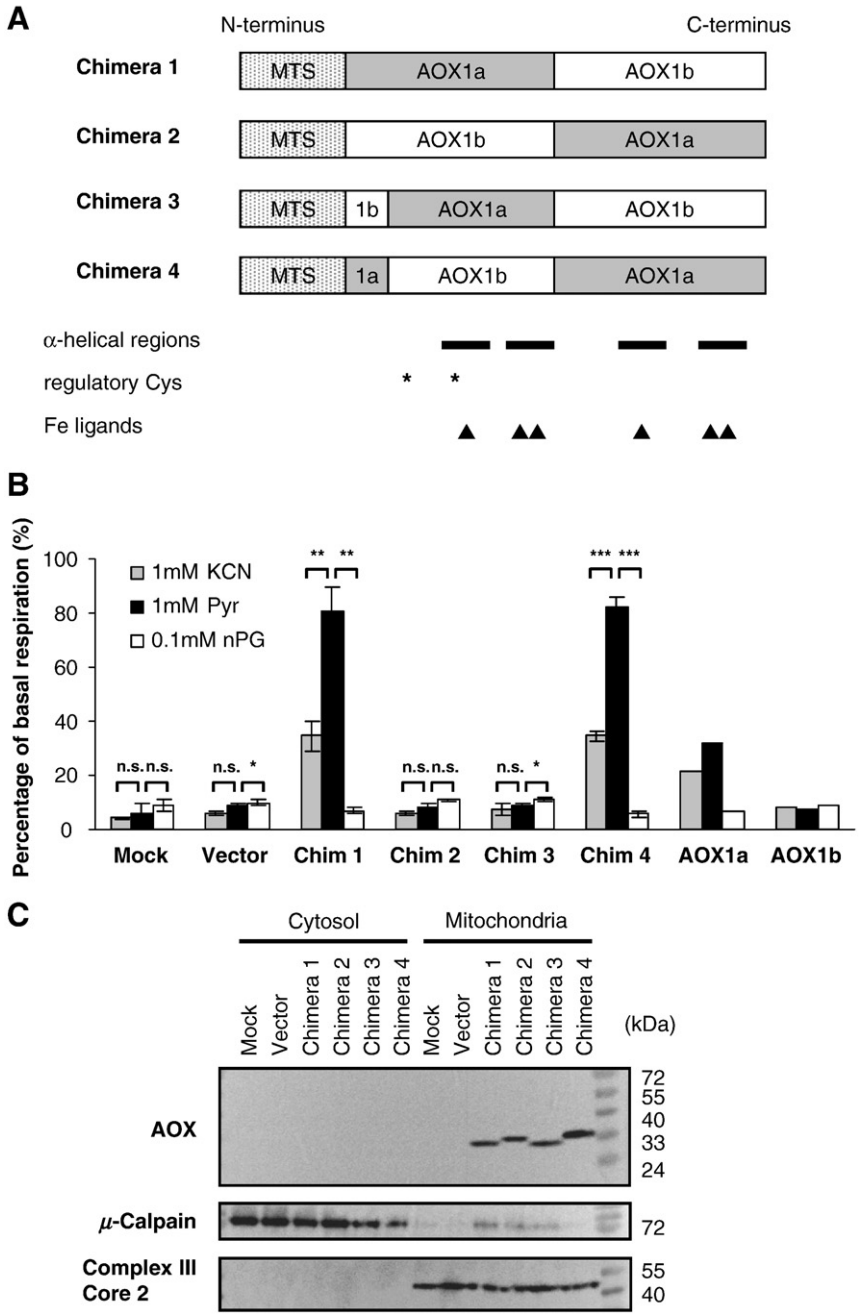


**Fig. 4.** Function and expression of chimeric AcoAOX proteins in HeLa cells. (A) Schematic representation of constructs that express the chimeric proteins. Sequences encoding AcoAOX1a and AcoAOX1b were partially substituted by their counterparts to cover whole sequences corresponding to the putative mature forms in their wild type. MTS represent the mitochondrial targeting sequence referred in Fig. 3. Relative positions for several structural features predicted for AcoAOX1a and AcoAOX1b are also indicated at the bottom of the figure as follows: black bars for α-helical region, asterisks for regulatory cysteines and arrowheads for iron binding ligands. (B) Respiratory capacities of non-treated HeLa cells (Mock) and those transfected with vector (Vector), the chimeric constructs (Chim1, 2, 3 and 4) and the two AOX constructs (AOX1a and AOX1b). The capacities were obtained by the method indicated in panel C of Fig. 3. The graph was created with data from three independent experiments for Mock, Vector, Chim 1, 2, 3, and 4 and a single experiment for AOX1a and AOX1b. The capacities of AOX1a and AOX1b resulted in the range of those shown in panel C of Fig. 3, indicating that they represent their typical responses to the drug additions. Significance of *t*-test is indicated as follows: $^{*}P<0.05$, $^{**}P<0.01$, $^{***}P<0.001$ and n.s. not significant. (C) Western blotting of subcellular fractions extracted from the HeLa cells. The samples were immunoblotted with the AOA monoclonal antibody as well as anti-μ-calpain antibody and anti-complex III core 2 subunit antibodies as described in panel D of Fig. 3. A protein standard is indicated at the right of the image along with the corresponding molecular mass in kDa.

cells behaved like the chimera 2-expressing cells and the empty vector control during the sequential additions of the drugs, the oxygen consumption pattern of chimera 4-expressing cells highly resembled that of chimera 1-expressing cells. The chimera 4 showed a high level of oxygen consumption in the presence of KCN followed by significant activation by pyruvate up to 237.6 ± 9.6% of the cyanide-resistant oxygen consumption level and its subsequent inhibition by nPG.

Expressions of the chimeric AOX proteins were also confirmed by Western blotting of the subcellular fractions from each transfectants (Fig. 4C). The results clearly show that all of the chimeric proteins were expressed at relatively equivalent level within the cells and were co-fractioned with the mitochondrial marker protein rather than the cytosolic marker protein. This indicates that the chimeric proteins were successfully expressed and localized in a similar fashion to their original proteins. Molecular masses of the proteins were variable,

however, and could be categorized into two groups. Chimera 1 and chimera 3 were detected between 34 to 35 kDa, as was the case with AcoAOX1b, whereas signals of chimera 2 and chimera 4 appeared between 32 to 33 kDa, similar to that of AcoAOX1a.

### 3.5. Relative quantification of AcoAOX1a and AcoAOX1b in appendix tissues

Since cDNAs encoding the active (*AcoAOX1a*) and inactive (*AcoAOX1b*) AOX isoforms had been isolated from the same thermogenic appendices, expression quantities and patterns of their transcripts in the tissue was of great interest to us. Therefore, quantitative expression analysis of *AcoAOX1a* and *AcoAOX1b* was performed for the appendices from pre-thermogenic, thermogenic and post-thermogenic stages using cycling probe technology in real-time PCR, which is a method specialized for detecting a single polymorphism of nucleotide sequences with high specificity [24,25] (Fig. S2).

Our analyses revealed coexpression of the two AOX transcripts in appendices from all of the stages, but AcoAOX1a was expressed significantly higher in the thermogenic tissue (Fig. 5). The expression level of *AcoAOX1a* in the thermogenic appendix was $7.9 \pm 3.1$ times as high as that of *AcoAOX1b*. Following the time course of thermogenesis, the expression level of *AcoAOX1a* was up-regulated significantly in the thermogenic stage, being $18.4 \pm 3.4$ and $12.8 \pm 5.3$ times the level of that in the pre-thermogenic and post-thermogenic stages, respectively. In the case of *AcoAOX1b*, there was a similar tendency, but without statistical significance.

## 4. Discussion

It has long been considered that AOX plays a key role in heat production of most thermogenic plants, in which its expression is up-regulated during thermogenesis. In fact, such molecular evidence has been presented in several species of the arum lily family (Araceae), including skunk cabbage (*Symplocarpus renifolius*) [31], voodoo lily (*S. guttatum*) [32], dragon lily (*D. vulgaris*) [20] and also in the non-arum, the sacred lotus (*N. nucifera*) [33], but not in any of the genus *Arum* despite its long history as a research interest. To reveal the molecular nature of AOX from an *Arum* species, we here report molecular characteristics of two full-length *AOX* cDNAs (Fig. 2) isolated from thermogenic appendices of *A. concinnatum*, a recently identified thermogenic species of the genus *Arum* [19] (Fig. 1).

Our study shows that two species of *AOX* transcripts, *AcoAOX1a* and *AcoAOX1b*, are coexpressed in thermogenic appendices of *A. concinnatum* (Figs. 2 and 5). The results presented in the quantitative expression analysis (Fig. 5) strongly suggest that neither *AcoAOX1a* nor *AcoAOX1b* was an artifact derived from PCR procedures because both transcripts were detected not only with gene-specific primers but also with probes that recognize single nucleotide polymorphisms (Fig. S2). Although both *AcoAOX1a* and *AcoAOX1b* showed expression patterns in agreement with a perception that increased *AOX* abundance is responsible for thermogenesis in plants, only *AcoAOX1a* should be considered as the major AOX involved in thermogenesis in the appendices of *A. concinnatum* due to a large disparity in their expression abundance (Fig. 5). Although results obtained from heterologous expression systems do not always reflect native behavior of an enzyme, our functional analyses, in which AcoAOX1b did not show any cellular respiration attributable to AOX activity (Fig. 3), also support that possibility.

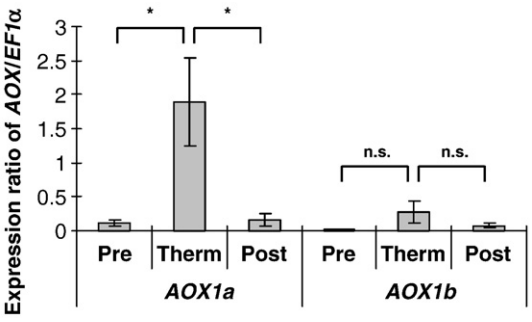


**Fig. 5.** Expression analysis of transcripts encoding *AcoAOX1a* and *AcoAOX1b* in appendix tissues collected from pre-thermogenic (Pre), thermogenic (Therm) and post-thermogenic (Post) stages. Transcript levels of the two *AcoAOXs* (*AOX1a* and *AOX1b*), as well as that of elongation factor 1α (*EF1α*), were quantified independently by standard curve methodology in real-time PCR. As absolute quantification of the targeted transcripts allowed the expression level of either *AOX* to be compared with that of its counterpart across the samples under normalization of initial cDNA amount, expression ratios of *AOX*/*EF1α* were calculated. Significance of *t*-test is indicated as follows: $*P<0.05$ and n.s. not significant.

By taking a mutagenic approach with chimeric proteins of AcoAOXs, we have identified that a non-synonymous amino acid substitution of E83K is responsible for the loss of activity in AcoAOX1b (Fig. 4). Although there have been no reports of functional alteration caused by a substitution on the N-terminal region of AOX except for CysI, an allelic variation of *Oryza sativa* AOX1a (OsAOX1a) with a non-synonymous substitution in the neighborhood of E83K was demonstrated to affect mobility of the proteins in SDS-PAGE [34], giving us a suspicion that there could also be a similar inactive AOX in rice. In fact, distribution of these alleles is tightly linked to a presence of the quantitative trait locus (QTL) for low temperature tolerance among rice varieties, and varieties without the QTL conserve lysine at the substation site instead of asparagine of those with the QTL [34].

The E83K substitution is located on the structurally undefined N-terminal region (Fig. 6A). Since comparative modeling for the N-terminal region of AOX has not been reported to date, this region has often been considered independently from the structurally defined α-helical bundle whenever structure–function relationships are discussed. However, our results present new perspectives on structure–function relationships of the N-terminal region of AOX and possible interpretations for effect of E83K at the molecular level.

We postulate first of all that tertiary structure is present in the N-terminal region of AOX, and that it comes close enough to the α-helical bundle to establish functional relationships between them. It may be that arrangement of the substitution site in spatial proximity to the catalytic α-helical bundle allows E83 of AcoAOX1a or K83 of AcoAOX1b to interact directly with the active center or other crucial residues in the vicinity. Indeed, the substitution site lies at the position seventy-eight residues upstream from the beginning of the first α-helix region, which would be an unreasonable distance if it functions effectively on the active center without forming any tertiary structure. On the basis of its primary structure, the same discrepancy holds true for the CysI site, which is still separated by forty-eight residues from the first α-helix region. Thus, it seems logical to presume that there exists tertiary structural complexity in the N-terminal region of AOX.

Apart from direct interactions of E83 or K83 with a catalytic component of AOX, a charge-induced conformational change could cause the loss of function in AcoAOX1b. This event has been proposed as a candidate mechanism by which α-keto acids activate the AOX [35], and a charged moiety of thiohemiacetal adduct at the sulfhydryl group of CysI has been regarded as an initial trigger in that process [11,35]. Since such a highly specified local distribution of a charged component on the N-terminal region has a drastic impact on the AOX activity, it seems likely that the crucial conversion of a charged moiety would cause a conformational change to occur in the vicinity of K83 of AcoAOX1b, where a negatively charged carboxyl group is substituted by a positively charged amino group.

Sequence alignment of the N-terminal region of functionally characterized plant AOXs (Fig. 6B) has also offered new insights into the intramolecular effect of E83K. Because the N-terminal sequences of AOX are scarcely conserved across the genera or even the species,

A

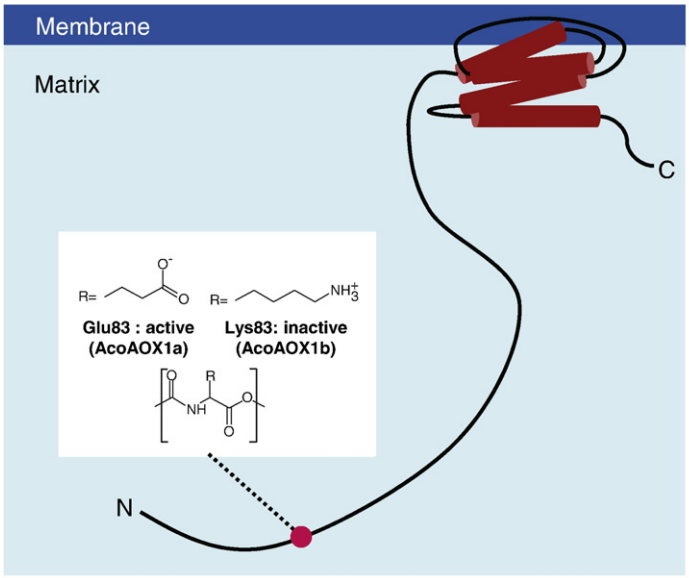


B

```
AcoAOX1a   STLSDPAQDGGKEKA---GTA-GEVPPGEGGAEQ----KAVV-SYWGVPP
AcoAOX1b   STLSDPAQDGGKEKA---GTA-GKVPPGEGGAEQ----KAVV-SYWGVPP
SgAOX      STLSARAQDGGKEKAA--GTA-GKVPPGEDGGAE----KEAVVSYWAVPP
SrAOX      STLSAPLAVAGEEKE---GKKA-EVAAPKAGARVED--KAVV-SHWGIPP

StAOX      STMSAPAAPEGETAA---KGDVDVTKKAEGDTEQ----KAVV-SYWGVPP
NtAOX1     SMALNDKQHDKKAEN---GSA--AATGGGDGGDE----KSVV-SYWGVQP
LeAOX1a    STAALNDKQQEKESSDKKVENTATATAAVNGGVG----KSVV-SYWGVPP
LeAOX1b    SNMNTSSKT--KEEQKTHNQPSHTDATNAAGDKA----KKIV-SYWGVDP
AtAOX1a    STITLGEKTPMKEEDANQKKTENESTGGDAAGGNNKGDKGIA-SYWGVEP
```

**Fig. 6.** Dynamic and diverse structure of the N-terminus of mature AOXs. (A) Schematic representation of AcoAOX structure as predicted by the current AOX model [7]. Cylinders represent the four α-helical structures. Position of the crucial substitution that is responsible for gain or loss of activity in AcoAOXs is indicated with a red circle. Side chains of the substituted amino acids are shown in a white box. (B) Sequence alignment of N-terminal region of mature AOXs whose functional characteristics have been analyzed and reported to date: *Sauromatum guttatum* AOX (SgAOX; P22185), *Symplocarpus renifolius* AOX (SrAOX; BAD83866.1), *Solanum tuberosum* AOX (StAOX; 2208475A), *Nicotiana tabacum* AOX1 (NtAOX1; Q41224.1), *Lycopersicon esculentum* AOX1a (LeAOX1a; AAK58482.1), *L. esculentum* AOX1b (LeAOX1b; AAK58483.1) and *A. thaliana* AOX1a (AtAOX; NP_188876.1). Amino acid sequences are aligned from the conserved serine near the cleavage site of mitochondrial targeting sequence to the beginning of homologous region downstream of the conserved SXW motif, which correspond to the sequence from S64 to P86 in AcoAOXs. Blue bold characters represent conserved residues, and red bold characters represent residues corresponding to the 83rd amino acids of AcoAOXs.

no residues corresponding to E83 or K83 of AcoAOXs could be identified in most AOXs, except for SgAOX and SrAOX, which are from the same family (Araceae) as *A. concinnatum*. SrAOX is reported to show cyanide-resistant, nPG-sensitive and pyruvate-inducible activity [36], as is the case with AcoAOX1a, thus it seems reasonable for the enzyme to possess glutamic acid at the position. On the other hand, SgAOX, which functions in a constitutively active fashion [37], has lysine at the corresponding site. This fact strongly indicates that appearance of lysine at the position alone is not sufficient for loss of function in AOX, and suggests it rather works in coordination with one or more residues to influence the AOX activity. A subject for future consideration may be to examine whether the lysine of SgAOX has any consequence on its constitutively active nature or not.

The physiological significance of catalytically inactive AcoAOX1b is an intriguing matter. Recently, Pils and Schultz predicted a number of potential inactive enzymes based on in silico analyses across metazoan genomes [38], and in fact, some catalytically inactive enzymes have been reported to function in post-translational regulation of their active counterparts [39]. For instance, while the sequence and molecular structure of a copper chaperone for superoxide dismutase (CCS) is similar to that of superoxide dismutase (SOD1) itself, CCS does not show SOD1-like enzymatic activity, but regulates SOD1 through forming a heterodimer [39,40]. It seems to be possible that AcoAOX1b is selectively conserved for such a regulatory purpose or is merely being lost slowly under little selective pressure.

In summary, our study has shown that a single amino acid substitution in the structurally undefined N-terminal region can determine whether AcoAOX proteins are active or inactive in HeLa cells and has given us a hint that the N-terminal region of AOX possesses functional sites and a more dynamic nature than was previously considered. The recent increase in the number of AOX-encoding transcripts on accessible databases has resulted in speculation about their enzymatic properties, but these have not been elucidated. We suggest that functional analyses of the translation products are inevitably required to fairly evaluate characteristics of the respective AOXs as well as to explore novel molecular features of AOX.

## Acknowledgements

We thank Dr. Stergios Pirintsos for his support in our research in Crete, Greece. We are grateful to Robin Seymour, Kazushige Matsukawa, Yuka Ito and Akiko Takou for their assistance. This work was supported by the 21st Century COE program from the Japan

Society for the Promotion of Science and the Australian Research Council (DP 0771854).

## Appendix A. Supplementary data

Supplementary data associated with this article can be found, in the online version, at doi:10.1016/j.bbabio.2009.07.006.

## References

[1] A.E. McDonald, Alternative oxidase: an inter-kingdom perspective on the function and regulation of this broadly distributed 'cyanide-resistant' terminal oxidase, Func. Plant Biol. 35 (2008) 535–552.
[2] A.M. Wagner, K. Krab, M.J. Wagner, A.L. Moore, Regulation of thermogenesis in flowering Araceae: the role of the alternative oxidase, Biochim. Biophys. Acta 1777 (2008) 993–1000.
[3] D.P. Maxwell, Y. Wang, L. McIntosh, The alternative oxidase lowers mitochondrial reactive oxygen production in plant cells, Proc. Natl. Acad. Sci. U. S. A. 96 (1999) 8271–8276.
[4] K. Matsukawa, T. Kamata, K. Ito, Functional expression of plant alternative oxidase decreases antimycin A-induced reactive oxygen species production in human cells, FEBS Lett. 583 (2009) 148–152.
[5] H. Lambers, Cyanide-resistant respiration: a non-phosphorylating electron transport pathway acting as an energy overflow, Physiol. Plant. 55 (1982) 478–485.
[6] J.R. Watling, S.A. Robinson, R.S. Seymour, Contribution of the alternative pathway to respiration during thermogenesis in flowers of the sacred lotus, Plant Physiol. 140 (2006) 1367–1373.
[7] M.E. Andersson, P. Nordlund, A revised model of the active site of alternative oxidase, FEBS Lett. 449 (1999) 17–22.
[8] M.S. Albury, C. Affourtit, A.L. Moore, A highly conserved glutamate residue (Glu-270) is essential for plant alternative oxidase activity, J. Biol. Chem. 273 (1998) 30301–30305.
[9] M.S. Albury, C. Affourtit, P.G. Crichton, A.L. Moore, Structure of the plant alternative oxidase, J. Biol. Chem. 277 (2002) 1190–1194.
[10] D.A. Berthold, M.E. Andersson, P. Nordlund, New insight into the structure and function of the alternative oxidase, Biochim. Biophys. Acta 1460 (2000) 241–254.
[11] D.M. Rhoads, A.L. Umbach, C.R. Sweet, A.M. Lennon, G.S. Rauch, J.N. Siedow, Regulation of the cyanide-resistant alternative oxidase of plant mitochondria, J. Biol. Chem. 273 (1998) 30750–30756.
[12] J.N. Siedow, A.L. Umbach, The mitochondrial cyanide-resistant oxidase: structural conservation amid regulatory diversity, Biochim. Biophys. Acta 1459 (2000) 432–439.
[13] A.L. Umbach, V.S. Ng, J.N. Siedow, Regulation of plant alternative oxidase activity: a tale of two cysteines, Biochim. Biophys. Acta 1757 (2006) 135–142.
[14] I. Djajanegara, R. Holtzapffel, P.M. Finnegan, M.H.N. Hoefnagel, D.A. Berthold, J.T. Wiskich, D.A. Day, A single amino acid change in the plant alternative oxidase alters the specificity of organic acid activation, FEBS Lett. 454 (1999) 220–224.
[15] R.C. Holtzapffel, J. Castelli, P.M. Finnegan, A.H. Millar, J. Whelan, D.A. Day, A tomato alternative oxidase protein with altered regulatory properties, Biochim. Biophys. Acta 1606 (2003) 153–162.
[16] D.A. Berthold, Isolation of mutants of the *Arabidopsis thaliana* alternative oxidase (ubiquinol:oxygene oxidoreductase) resistant to salicylhydroxamic acid, Biochim. Biophys. Acta 1364 (1998) 73–83.
[17] A.L. Moore, M.S. Albury, Further insights into the structure of the alternative oxidase: from plants to parasites, Biochem. Soc. Trans. 36 (2008) 1022–1026.
[18] K. Nakamura, K. Sakamoto, Y. Kido, Y. Fujimoto, T. Suzuki, M. Suzuki, Y. Yabu, N. Ohta, A. Tsuda, M. Onuma, K. Kita, Mutational analysis of the *Trypanosoma vivax* alternative oxidase: the $E(X)_6Y$ motif is conserved in both mitochondrial alternative oxidase and plastid terminal oxidase and is indispensable for enzyme activity, Biochem. Biophys. Res. Commun. 334 (2005) 593–600.
[19] R.S. Seymour, M. Gibernau, S.A. Pirintsos, Thermogenesis of three species of *Arum* from Crete, Plant Cell Environ. 32 (2009) 1467–1476.
[20] K. Ito, R.S. Seymour, Expression of uncoupling protein and alternative oxidase depends on lipid or carbohydrate substrates in thermogenic plants, Biol. Lett. 1 (2005) 427–430.
[21] D.M. Rhoads, L. McIntosh, Isolation and characterization of a cDNA clone encoding an alternative oxidase protein of *Sauromatum guttatum* (Schott), Proc. Natl. Acad. Sci. U. S. A. 88 (1991) 2122–2126.
[22] K. Tamura, J. Dudley, M. Nei, S. Kumar, MEGA4: Molecular Evolutionary Genetics Analysis (MEGA) software version 4.0. Mol. Biol. Evol. 24 (2007) 1596–1599.
[23] M.G. Claros, Mitoprot, a Macintosh application for studying mitochondrial proteins, Comput. Appl. Biosci. 11 (1995) 441–447.
[24] P. Duck, G. Alvarado-Urbina, B. Burdick, B. Collier, Probe amplifier system based on chimeric cycling oligonucleotides, BioTechniques 9 (1990) 142–148.
[25] F. Bekkaoui, I. Poisson, W. Crosby, L. Cloney, P. Duck, Cycling probe technology with RNase H attached to an oligonucleotide, BioTechniques 20 (1996) 240–248.
[26] E. Bermadinger-Stabentheiner, A. Stabentheiner, Dynamics of thermogenesis and structure of epidermal tissues in inflorescences of *Arum maculatum*, New Phytol. 131 (1995) 41–50.
[27] D. Barabé, C. Lacroix, M. Gibernau, Development of the flower and inflorescence of *Arum italicum* (Araceae), Can. J. Bot. 81 (2003) 622–632.
[28] M. Gibernau, D. Macquart, G. Przetak, Pollination in the genus *Arum*, Aroideana 27 (2004) 148–166.
[29] T.E. Elthon, R.L. Nickels, L. McIntosh, Monoclonal antibodies to the alternative oxidase of higher plant mitochondria, Plant Physiol. 89 (1989) 1311–1317.
[30] P.M. Finnegan, A.R. Wooding, D.A. Day, An alternative oxidase monoclonal antibody recognizes a highly conserved sequence among alternative oxidase subunits, FEBS Lett. 447 (1999) 21–24.
[31] Y. Onda, Y. Kato, Y. Abe, T. Ito, M. Morohashi, Y. Ito, M. Ichikawa, K. Matsukawa, Y. Kakizaki, H. Koiwa, K. Ito, Functional coexpression of the mitochondrial alternative oxidase and uncoupling protein underlies thermoregulation in the thermogenic florets of skunk cabbage, Plant Physiol. 146 (2008) 636–645.
[32] T.E. Elthon, L. McIntosh, Identification of the alternative oxidase of higher plant mitochondria, Proc. Natl. Acad. Sci. U. S. A. 84 (1987) 8399–8403.
[33] N.M. Grant, R.E. Miller, J.R. Watling, S.A. Robinson, Synchronicity of thermogenic activity, alternative pathway respiratory flux, AOX protein content, and carbohydrates in receptacle tissues of sacred lotus during floral development, J. Exp. Bot. 59 (2008) 705–714.
[34] F. Abe, K. Saito, K. Miura, K. Toriyama, A single nucleotide polymorphism in the alternative oxidase gene among rice varieties differing in low temperature tolerance, FEBS Lett. 527 (2002) 181–185.
[35] A.L. Umbach, J.N. Siedow, The reaction of soybean cotyledon mitochondrial cyanide-resistant oxidase with sulfhydryl reagents suggests that α-keto acid activation involves the formation of a thiohemiacetal, J. Biol. Chem. 271 (1996) 25019–25026.
[36] Y. Onda, Y. Kato, Y. Abe, T. Ito, Y. Ito-Inaba, M. Morohashi, Y. Ito, M. Ichikawa, K. Matsukawa, M. Otsuka, H. Koiwa, K. Ito, Pyruvate-sensitive AOX exists as a non-covalently associated dimer in the homeothermic spadix of the skunk cabbage, *Symplocarpus renifoelius*, FEBS Lett. 581 (2007) 5852–5858.
[37] P.G. Crichton, C. Affourtit, M.S. Albury, J.E. Carre, A.L. Moore, Constitutive activity of *Sauromatum guttatum* alternative oxidase in *Schizosaccharomyces pombe* implicates residues in addition to conserved cysteines in α-keto acid activation, FEBS Lett. 579 (2005) 331–336.
[38] B. Pils, J. Schultz, Inactive enzyme-homologues find new function in regulatory processes, J. Mol. Biol. 340 (2004) 399–404.
[39] G.J. Bartlett, N. Borkakoti, J.M. Thornton, Catalysing new reactions during evolution: economy of residues and mechanism, J. Mol. Biol. 331 (2003) 829–860.
[40] A.L. Lamb, A.S. Torres, T.V. O'Halloran, A.C. Rosenzweig, Heterodimer formation between superoxide dismutase and its copper chaperone, Biochemistry 39 (2000) 14720–14727.